
SCIAMACHY Absorbing Aerosol Index

Algorithm Theoretical Basis Document

Author : L.G. Tilstra

Doc. nr. : KNMI/SC-AAI/ATBD/01

Issue : 2.0

Date : 11-10-2011



Document status sheet

Issue	Date	Page(s)	Modified Items / Reason for Change
0.1	09-07-2007	all	first draft version
0.2	17-12-2007	all	second draft; added table and figures, completed document
0.3	24-01-2008	all	first revised version
0.4	07-10-2008	all	second revised version; updated Sections 3, 4, and 5
1.0	02-09-2009	all	new version after major algorithm update (to version 4.1)
1.1	14-10-2009	all	minor update of Section 5.1
1.2	22-01-2010	all	minimal changes after release of v4.1 data
2.0	11-10-2011	all	update to algorithm version 5.0; new degradation correction

Contents

1	Introduction	5
1.1	Document purpose and scope	5
1.2	Definition of viewing and solar angles	5
1.3	Calibration of the level-1 files	5
1.4	Suggested reading material	7
1.5	Abbreviations and acronyms	7
2	Definition of the Absorbing Aerosol Index	9
2.1	Definition of the residue	9
2.2	Definition of the AAI	10
2.3	Interpretation and meaning of the AAI	10
3	Calculation of the residue	11
3.1	Algorithm setup	11
3.2	Look-up tables	12
3.3	Reflectance	13
3.4	Geometry corrections	13
3.5	Ozone absorption	13
3.6	Surface height	13
4	Error analysis of the residue	16
4.1	Calibration correction	16
4.2	Correction for obstruction in the FOV for westernmost pixels	16
4.3	Correction for instrument degradation	17

5	Filtering and flagging	20
5.1	Integration time	20
5.2	Backscan pixels	21
5.3	Solar zenith angle	21
5.4	Sunglint situations	21
5.5	Solar eclipse events	22
5.6	Reflectances and residues	22
5.7	Quality flags	22
A	Readme file delivered with look-up tables	24
B	Overview of solar eclipse events	27

1 Introduction

1.1 Document purpose and scope

This document is the Algorithm Theoretical Basis Document for the SC-AAI, the Absorbing Aerosol Index (AAI) developed at our two institutes. The aim of this ATBD is to present the scientific background of the algorithm, to provide a description of the actual algorithm setup, and to explain the machinery behind the SC-AAI data we provide at the TEMIS website (<http://www.temis.nl>).

It is assumed that the reader has some basic knowledge of the SCIAMACHY instrument [1] and of the way it performs its nadir measurements. If needed, additional background information on the subject can be found in the SCIAMACHY level 0-1c processing ATBD [2].

1.2 Definition of viewing and solar angles

The sphere in Figure 1 defines, in a graphical way, the angles that are used to specify the viewing and solar directions of the incoming and outgoing radiation. An imaginary volume element, responsible for the scattering of incident sunlight, is located in the origin of the sphere. The solar direction is described by the solar zenith angle θ_0 and the solar azimuth angle ϕ_0 . Likewise, the viewing direction is characterised by the viewing zenith angle θ and the viewing azimuth angle ϕ .

In this ATBD we make use of a right-handed coordinate frame, meaning that $\phi - \phi_0$ as sketched in Figure 1 is positive. By doing this, we follow the same definition of ϕ and ϕ_0 adopted for official SCIAMACHY data. However, there is no real need to specify this sense of rotation, because the sign of the azimuth difference $\phi - \phi_0$ is not relevant. For completeness, we mention that the single scattering angle, following this definition of angles, is calculated from the following formula:

$$\cos \Theta = -\cos \theta \cos \theta_0 + \sin \theta \sin \theta_0 \cos (\phi - \phi_0) \quad (1)$$

The viewing and solar angles that are used by the AAI retrieval code are given w.r.t. sea level and correspond to the middle of the integration time of a measurement footprint. The angles may be calculated from the angles provided in the SCIAMACHY level-1c product (see Section 3.4).

1.3 Calibration of the level-1 files

The calibration of SCIAMACHY level-1b files into SCIAMACHY level-1c files is performed by `scia_n11`, a calibration tool that is part of the NADC tools [3]. We try to use the most recent and stable version that is available. At the time of writing, this was version 1.2.0. This version is able to perform a correction for instrument degradation using so-called m-factor correction factors [4].

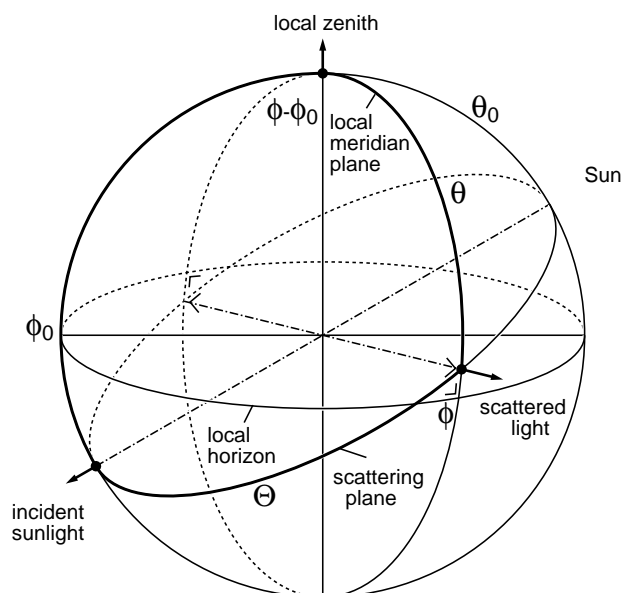


Figure 1: Definition of the solar and viewing angles as used in this ATBD. The single scattering angle is denoted by Θ , and is calculated using Eq. 1.

When running `scia_n11`, the following switches are set:

```
-nadir          extract Nadir MDS records
-no_gads        do not extract Global Annotation Data Sets (GADS)
-no_ads         do not extract Annotation Data Sets (ADS)
-no_aux0        do not extract Auxiliary ADS records
-no_pmd0        do not extract PMD ADS records
-no_pmd         do not extract PMD MDS records
-no_polV        do not extract fractional polarisation MDS
```

The following options are passed on to `scia_n11`:

```
--clus=9
--cal=0m,1,2,3,4,5,6,7,8,9
```

The switch `-nadir` is given to only process nadir states. Using this switch also includes the so-called ‘nadir static’ and ‘narrow swath’ monitoring states in the resulting level-1c file. By the specification of the option `--clus=9` only data for spectral cluster 9 are stored in the level-1c file. The calibration option `--cal=M`, which was used in the past to switch on the m-factor correction [4], is not used any more as of SC-AAI version 5.0. For an explanation of the other options, see reference [3].

1.4 Suggested reading material

The following paper describes the retrieval algorithm when applied to GOME [5] data, and analyses the quality of the data. A proper sensitivity study is also presented in this paper.

M. de Graaf, P. Stammes, O. Torres, and R. B. A. Koelemeijer, *Absorbing Aerosol Index: Sensitivity analysis, application to GOME and comparison with TOMS*, *J. Geophys. Res.* **110**, D01201, doi:10.1029/2004JD005178, 2005.

In the following paper, the algorithm is applied to SCIAMACHY data:

M. de Graaf and P. Stammes, *SCIAMACHY Absorbing Aerosol Index – calibration issues and global results from 2002-2004*, *Atmos. Chem. Phys.* **5**, 2385–2394, doi:10.5194/acp-5-2385-2005, 2005.

1.5 Abbreviations and acronyms

AAI	Absorbing Aerosol Index
ATBD	Algorithm Theoretical Basis Document
BBA	Biomass Burning Aerosols
DAK	Doubling-Adding KNMI
DDA	Desert Dust Aerosols
DOAS	Differential Optical Absorption Spectroscopy
DU	Dobson Units, 2.69×10^{16} molecules cm^{-2}
ENVISAT	Environmental Satellite
ERS	European Remote Sensing Satellite
ESA	European Space Agency
ETOPO-4	Topographic & Bathymetric dataset from the NGDC, 4 arc-min. resolution
FOV	Field-of-View
FRESCO	Fast Retrieval Scheme for Cloud Observables
GOME	Global Ozone Monitoring Experiment
IT	Integration Time
KNMI	Koninklijk Nederlands Meteorologisch Instituut (De Bilt, NL)
LUT	Look-Up Table
L2-AAI	Operational (level-2) Absorbing Aerosol Index product
MLS	Mid-Latitude Summer
NOAA	National Oceanic and Atmospheric Administration
NGDC	NOAA's National Geophysical Data Center (Boulder, Colorado, USA)

NL-SCIA-DC	Netherlands SCIAMACHY Data Center
NRT	Near-Real-Time
OMI	Ozone Monitoring Instrument
O3M SAF	Satellite Application Facility on Ozone Monitoring
PMD	Polarisation Measurement Device
PSD	Product Specification Document
RTM	Radiative Transfer Model
SBUV	Solar Backscatter Ultra-Violet radiometer
SC-AAI	SCIAMACHY Scientific Absorbing Aerosol Index product
SCIAMACHY	Scanning Imaging Absorption Spectrometer for Atmospheric Chartography
SLS	Spectral Light Source
SRON	Netherlands Institute for Space Research (Utrecht, NL)
SZA	Solar Zenith Angle
TEMIS	Tropospheric Emission Monitoring Internet Service (http://www.temis.nl)
TOA	Top-of-Atmosphere
TOMS	Total Ozone Mapping Spectrometer
TOSOMI	Total Ozone algorithm for SCIAMACHY using the OMI algorithm
UTC	Universal Time Co-ordinate
UV	Ultra-Violet
VIS	Visible
VZA	Viewing Zenith Angle
WLS	White Light Source

2 Definition of the Absorbing Aerosol Index

2.1 Definition of the residue

The Absorbing Aerosol Index (AAI) is a dimensionless quantity which was introduced to provide information about the presence of UV-absorbing aerosols in the Earth's atmosphere. It is derived directly from another quantity, the residue, which is defined by [6, 7]

$$r = -100 \cdot \left\{ {}^{10} \log \left(\frac{R_\lambda}{R_{\lambda_0}} \right)^{\text{obs}} - {}^{10} \log \left(\frac{R_\lambda}{R_{\lambda_0}} \right)^{\text{Ray}} \right\}. \quad (2)$$

In this equation, R_λ denotes the Earth's reflectance at wavelength λ . The superscript ^{obs} refers to reflectances which are measured by, in this case, SCIAMACHY, while the superscript ^{Ray} refers to modelled reflectances. These modelled reflectances are calculated for a cloud-free and aerosol-free atmosphere in which only Rayleigh scattering, absorption by molecules, Lambertian surface reflection as well as surface absorption can take place (cf. Section 3.2).

The reflectance, in this ATBD, is defined in the usual way as

$$R = \frac{\pi I}{\mu_0 E}, \quad (3)$$

where I is the radiance reflected by the Earth atmosphere (in $\text{Wm}^{-2}\text{nm}^{-1}\text{sr}^{-1}$), E is the incident solar irradiance at the top of the atmosphere perpendicular to the solar beam (in $\text{Wm}^{-2}\text{nm}^{-1}$), and μ_0 is the cosine of the solar zenith angle θ_0 . The wavelengths λ and λ_0 must lie in the UV, and were set to 340 and 380 nm, respectively, for the SCIAMACHY AAI retrieval.

The Rayleigh atmosphere in the simulations is bounded below by a Lambertian surface having a wavelength independent surface albedo A_s . The surface albedo A_s is, however, not meant to represent the actual ground albedo in any way. Its value is obtained from requiring that the simulated reflectance equals the measured reflectance at the calculation wavelength λ_0 :

$$R_{\lambda_0}^{\text{obs}} = R_{\lambda_0}^{\text{Ray}}(A_s) \quad (4)$$

The surface albedo A_s found in this way is used to calculate R_λ^{Ray} , so we basically assume that the surface albedo is constant over the wavelength interval $[\lambda, \lambda_0]$. In the UV, this is in fact a good approximation for most surface types [8]. Note that Eq. 2 can now be reduced to

$$r = -100 \cdot {}^{10} \log \left(\frac{R_\lambda^{\text{obs}}}{R_\lambda^{\text{Ray}}} \right). \quad (5)$$

The combination of Eqs. 4 and 5 is the basis of the retrieval algorithm described in this ATBD.

2.2 Definition of the AAI

The importance of the residue, as defined in the previous section, lies in its ability to effectively detect the presence of absorbing aerosols even in the presence of clouds. When a positive residue is found ($r > 0$), absorbing aerosols are certainly present in the observed scene. Negative or zero residues on the other hand ($r \leq 0$), suggest a definite absence of absorbing aerosols in the observed scene. For that reason, the AAI is traditionally defined as equal to the residue r where the residue is positive, while it is simply not defined where the residue has a negative value.

2.3 Interpretation and meaning of the AAI

Owing to its specific definition in the ultra-violet (UV) wavelength range, the residue method is only sensitive to UV-absorbing aerosols. In practice, these are mainly desert dust aerosols (DDA) and biomass burning aerosols (BBA). The BBA are usually created by forest fires, or by human combustion activities of a similar nature. The DDA have their origin in the Earth's desert regions.

As an example of this, Figure 2 presents a global map of the monthly mean SCIAMACHY AAI for June 2004. The large plume of UV-absorbing aerosols is called the "Global Dust Belt" [9]. These are dust aerosols, originating from various desert areas, which are transported westwards over the North Atlantic ocean. The most important desert regions that produce dust aerosols are indicated.

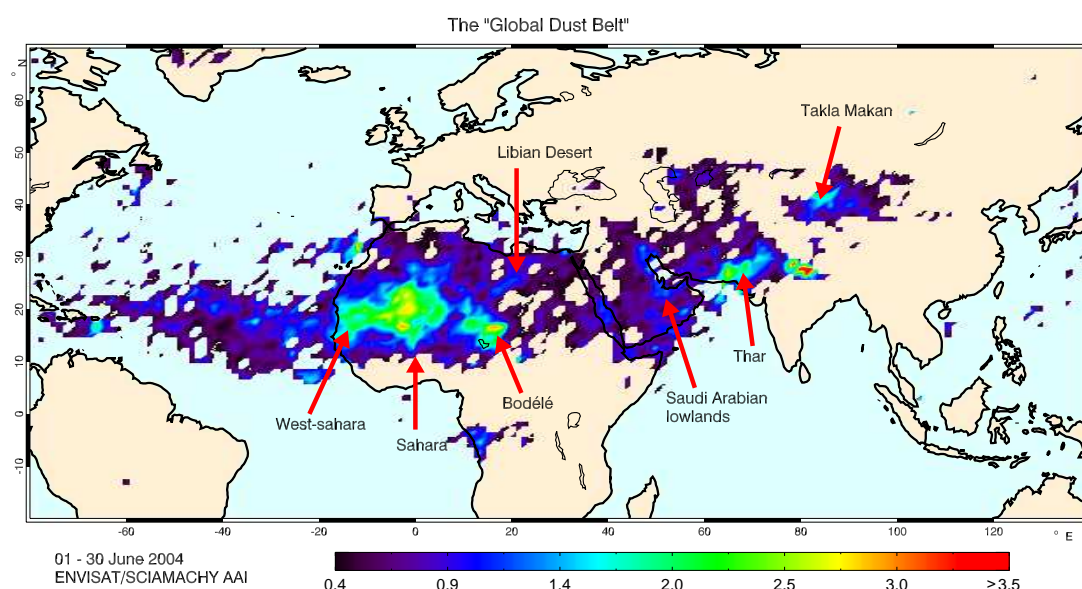


Figure 2: Global map of the monthly mean SCIAMACHY AAI for June 2004. The so-called "Global Dust Belt" is clearly visible, and illustrates the transport of desert dust aerosols (DDA) over the North Atlantic ocean. The picture was taken from reference [9], with consent of its author.

3 Calculation of the residue

3.1 Algorithm setup

The first step in the calculation of the residue involves finding the artificial surface albedo A_s for which the measured SCIAMACHY reflectance at the reference wavelength $\lambda_0 = 380$ nm equals the simulated Rayleigh reflectance at the same wavelength (cf. Eq. 4). The simulated reflectances are calculated using a set of look-up tables (LUTs). These LUTs are described in Section 3.2.

The simulations basically describe a cloud-free, homogeneous atmosphere which is bounded below by a Lambertian surface. The contribution of the surface to the TOA reflectance may be separated from that of the atmosphere according to the following formula [10]:

$$R^{\text{Ray}}(\mu, \mu_0, \phi - \phi_0, A_s) = R^0(\mu, \mu_0, \phi - \phi_0) + \frac{A_s T(\mu, \mu_0)}{1 - A_s s^*} \quad (6)$$

In this equation, the first term R^0 is the path reflectance, which is the atmospheric contribution to the reflectance. The second term is the contribution of the surface with an albedo A_s . The parameter T is the total atmospheric transmission for the given zenith angles, s^* is the spherical albedo of the atmosphere for illumination from below, μ is the cosine of the viewing zenith angle θ , and likewise, μ_0 is the cosine of the solar zenith angle θ_0 defined earlier in Section 1.2.

Using Eq. 6 and by demanding that the simulated Rayleigh reflectance $R_{\lambda_0}^{\text{Ray}}$ equals the measured reflectance $R_{\lambda_0}^{\text{obs}}$ at $\lambda_0 = 380$ nm, we find the following expression for the surface albedo A_s :

$$A_s = \frac{R_{\lambda_0}^{\text{obs}} - R_{\lambda_0}^0}{T_{\lambda_0}(\mu, \mu_0) + s_{\lambda_0}^*(R_{\lambda_0}^{\text{obs}} - R_{\lambda_0}^0)} \quad (7)$$

In this equation, $R_{\lambda_0}^0$ denotes the simulated (path) reflectance at wavelength λ_0 , calculated for the actual atmospheric situation, but without the surface reflection contribution. The path reflectance R^0 can of course be expanded in a Fourier series. In our case, with a simple Rayleigh atmosphere, this expansion is exact with only three terms in the azimuth angle difference $\phi - \phi_0$:

$$R^0 = a_0 + \sum_{i=1}^2 2a_i(\mu, \mu_0) \cos i(\phi - \phi_0) \quad (8)$$

The idea of the algorithm setup is that with proper LUTs of a_0 , a_1 , a_2 , T , and s^* , we can easily calculate $R_{\lambda_0}^0$, A_s , $R_{\lambda_0}^{\text{Ray}}$, and finally, the residue. The advantage of this approach is that both the azimuthal dependence and the dependence on surface albedo are treated analytically, and are therefore not part of the LUTs. Some interpolation over the remaining parameters is necessary. In this case we have to interpolate over μ and μ_0 , surface height h_s , and ozone column Ω .

3.2 Look-up tables

The look-up tables (LUTs) were created using the radiative transfer code DAK (which stands for “Doubling-Adding KNMI”, see reference [11]). This vector RTM takes polarisation into account, as well as ozone absorption and Lambertian surface reflection. As of version 4.1, a pseudo-spherical version of the RTM DAK was used. The version number of this DAK code was 3.1.1. The pseudo-sphericity leads to a symmetry breaking and a resulting change in the algorithm approach w.r.t. algorithm version 4.0, as described in, for instance, issue 0.4 of this ATBD. For more details on the pseudo-sphericity and the implications it has on the algorithm setup, please consult Appendix A. Also, as of version 4.1, O_2-O_2 absorption is included in the radiative transfer calculations of the LUTs. A fixed O_2 background concentration is used, which is a justified simplification.

The calculations at the two wavelengths λ and λ_0 were done for surface albedos $A_t = \{0.0, 0.5, 1.0\}$, for an azimuth difference $\phi - \phi_0 = 0^\circ$, for 42×42 combinations of the zenith angles μ and μ_0 , for cloud-free conditions in a standard Mid-Latitude Summer (MLS) atmosphere [12], for 7 ozone column values $\Omega = \{50, 200, 300, 350, 400, 500, 650\}$ DU, and for 9 surface heights h_s ranging from 0 to 8 km in 1 km steps. The variation of the surface height was achieved by removing an appropriate number of layers from the bottom of the model atmosphere. Such a removal of layers affects the ozone columns to a (very small) degree, which was compensated for by scaling the entire ozone profile in such a way that the original ozone column value was reinstated.

The coefficients a_0 , a_1 , and a_2 , as defined in Section 3.1, were delivered directly by the DAK code from the runs with albedo $A_t = 0$. The definition of the coefficients a_0 , a_1 , and a_2 is such that the path reflectance R^0 may be reconstructed from them according to

$$R^0 = a_0 + 2a_1 \cos(\phi - \phi_0) + 2a_2 \cos 2(\phi - \phi_0). \quad (9)$$

The parameters T and s^* were calculated from the reflectances $R_\lambda(\mu, \mu_0, 0, A_t)$, calculated for the three surface albedos A_t mentioned before, in combination with Eq. 6. This gives

$$s_\lambda^* = \frac{R_\lambda(\mu, \mu_0, 0, 1.0) - 2R_\lambda(\mu, \mu_0, 0, 0.5) + R_\lambda(\mu, \mu_0, 0, 0.0)}{R_\lambda(\mu, \mu_0, 0, 1.0) - R_\lambda(\mu, \mu_0, 0, 0.5)}, \quad (10)$$

independent on μ and μ_0 , dependent on surface height h_s , ozone column Ω and wavelength λ , and

$$T_\lambda(\mu, \mu_0) = (1 - s_\lambda^*) \cdot (R_\lambda(\mu, \mu_0, 0, 1.0) - R_\lambda(\mu, \mu_0, 0, 0.0)), \quad (11)$$

which is dependent on μ and μ_0 , surface height h_s , ozone column Ω , and wavelength λ . The LUTs for each of the two wavelengths contain the parameters a_0 , a_1 , a_2 , T , and s^* . All parameters except s^* are prepared as a function of μ and μ_0 , surface height, and ozone column. The parameter s^* does not depend on μ and μ_0 , and is given as a function of surface height and ozone column.

3.3 Reflectance

The reflectances R_{λ}^{obs} and $R_{\lambda_0}^{\text{obs}}$ are determined in the following manner. First the reflectance is calculated for all detector pixels in cluster 9 (320–391 nm). Then we identify those detector pixels that lie within the wavelength ranges $[\lambda - \omega, \lambda + \omega]$ and $[\lambda_0 - \omega, \lambda_0 + \omega]$, respectively, where $2\omega = 1.0$ nm. The reflectances of these detector pixels are then averaged, after which we obtain the band reflectances R_{λ}^{obs} and $R_{\lambda_0}^{\text{obs}}$. Note that $\lambda = 340$ nm, $\lambda_0 = 380$ nm.

3.4 Geometry corrections

The viewing and solar angles that are provided in the SCIAMACHY level-1b (and level-1c) product are given w.r.t. a height of 100 km above sea level. This is not a realistic reference height because most of the scattering takes place in the lower parts of the atmosphere. For that reason, we recalculate the SCIAMACHY viewing and solar angles w.r.t. sea level using the recipe given in reference [15]. The value of the Earth radius is taken from the level-1c product. The angles that are recalculated are the viewing zenith angle θ , the solar zenith angle θ_0 , and the relative azimuth difference $\phi - \phi_0$.

3.5 Ozone absorption

Ozone absorption is taken into account, and simulated LUT-reflectances for 7 different ozone column values are available for the interpolation mentioned in Section 3.1. However, the shape of the ozone profile is a fixed one. It was taken from the standard MLS atmospheric profile [12], which is used for all seasons and for all latitudes. Note that the sensitivity of the reflectance to the shape of the ozone profile at 340/380 nm is much less important than the sensitivity to the ozone column [14].

The ozone columns are taken from the SCIAMACHY TOSOMI total ozone product. Note that the TOSOMI data originate from the same SCIAMACHY cluster as the two wavelengths λ_0 and λ_1 . This ensures a perfect match in both footprint and time of measurement. If for some reason the total ozone columns are not available, SCIAMACHY assimilated ozone columns are available as a backup.

3.6 Surface height

The average surface height over the SCIAMACHY footprints is calculated using a surface height database. This surface height database was constructed from an ETOPO-4 elevation database [13], and has an angular resolution of 4 arc-minutes, which is sufficient for the task at hand. As we are only interested in the topographic information, all bathymetric information was removed from the database, and replaced by a zero surface height. See Figure 3 for a graphical explanation.

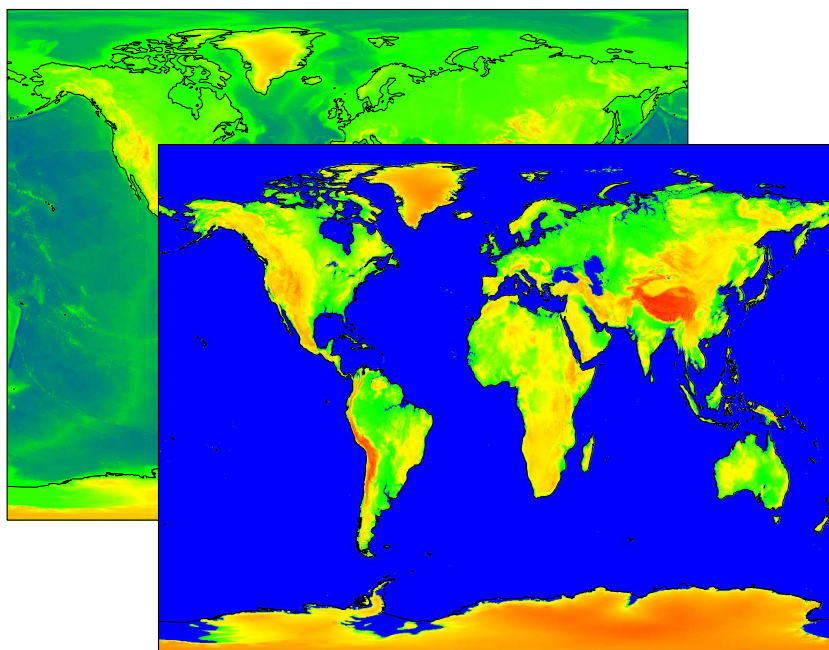


Figure 3: Image of the ETOPO-4 surface height database that was used (upper plot layer). This surface height database was constructed from an ETOPO-4 elevation database (lower plot layer in the figure). The resolution (cell size) of the surface height database is 4 arc-minutes.

The mean surface height for the footprint in question is calculated by first determining the grid points of the surface height database that fall inside the footprint, and then averaging their associated surface heights. With the moderate resolution offered by the ETOPO-4 based database, a SCIAMACHY footprint contains about 40–200 grid points, depending on the IT, the latitude, and whether the pixel is a so-called backscan pixel or not. In any case, the number of grid points inside the SCIAMACHY footprint is more than adequate for finding an accurate value for the mean surface height.

This was at least the result from tests with ETOPO-2, ETOPO-4, and ETOPO-10 databases. We processed SCIAMACHY orbit 2508, which largely covers land, using the beforementioned databases, and compared the surface height and residue for the pixels over land. With respect to the ETOPO-2 run, the ETOPO-4 run showed only small deviations in the surface height over land, with a standard deviation of 7.8 m, and a maximum deviation of 70.3 m. The ETOPO-10 run, however, showed a standard deviation of 48.0 m and a maximum deviation of 499.4 m.

The maximum absolute effect on the residue, caused by the maximum deviation in surface height w.r.t. the surface height of the ETOPO-2 run, was 0.07 (for the ETOPO-4 run) versus 0.49 (ETOPO-10 run). In other words, the ETOPO-4 database should be accurate enough for the job. (Using the ETOPO-2 database is of course the most accurate, but demands some more computational power.)

In the algorithm, we collect the ETOPO surface height grid points that fall within the polygon formed by the four corners of the SCIAMACHY footprint. The order in which the corner longitudes and latitudes are given is of course important, as illustrated by Figure 4. The order shown in (a) is the one adopted in the SCIAMACHY level-1c product; the order given in (b) is the one that is used in our retrieval algorithm. The latter order (b) is also the order in which the corner coordinates are provided in the SC-AAI level-2 data that are available on the TEMIS website.

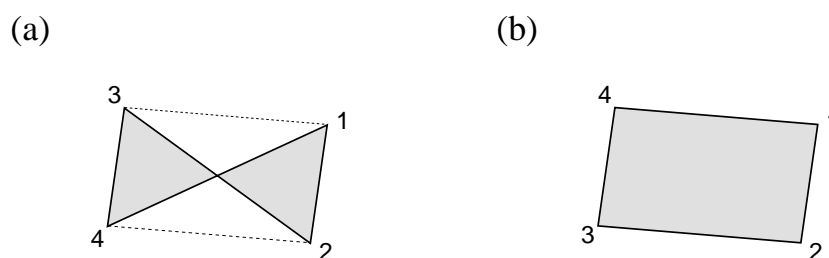


Figure 4: The order in which the corner points are given is important. The order shown in (a) is the one given in the SCIAMACHY level-1c product. The order in (b) is the one we have adopted in our algorithm, and provide in the SC-AAI data on the TEMIS website.

4 Error analysis of the residue

4.1 Calibration correction

A correct absolute calibration of the reflectance is really an essential ingredient for obtaining reliable AAI data. SCIAMACHY was after launch found to be underestimating the reflectance by typically 10–20% of its value in the UV. In our SC-AAI retrieval algorithm, the reflectances at 340 and 380 nm are therefore first multiplied by correction factors c_{340} and c_{380} , respectively.

For level-1 software versions up to 5.04, these correction factors were determined to be $c_{340} = 1.20$ and $c_{380} = 1.13$. Data with data processor software version 6.01 are not processed, because of the severe product errors that trouble this specific data version. As of software version 6.02, which is equipped with a new set of key data for the absolute radiometric calibration, the correction factors are considerably smaller and found to be equal to $c_{340} = 1.008$ and $c_{380} = 0.989$.

These correction factors were determined from a study in which the SCIAMACHY reflectance in the UV was compared with the reflectance calculated by the radiative transfer code DAK [14]. To have some idea about the impact of these correction factors, we recall [16] that the effect of these two correction factors may be approximated by the simple formula

$$\Delta r \approx -100 \cdot 10 \log\left(\frac{c_{340}}{c_{380}}\right). \quad (12)$$

When we fill in the appropriate corrections factors, the formula tells us that the residue of the current operational level-2 product (L2-AAI), which is not being corrected for the radiometric calibration problem, is on average 2.6 index points higher than the SC-AAI for data versions up to 5.04, and roughly 0.8 index points higher than the SC-AAI for data version 6.02 and higher.

4.2 Correction for obstruction in the FOV for westernmost pixels

This obstruction in the FOV was an issue until orbit 5656 of March 31, 2003, and resulted in slightly reduced signals for the westernmost measurements inside a scan. The problem was reported at the end of the year 2002 [17] and was solved by letting SCIAMACHY add an offset α_0 of magnitude 2.0° to the formerly assumed scan mirror positions. As a result of this, the swath of the instrument was shifted a bit towards the east. The value of α_0 was reduced to 1.0° around April 7, 2003, as this value turned out to be already enough to completely avoid the obstruction in the FOV.

Figure 5 illustrates the effect of the reduced signals on the residue in a graphical way. On the vertical axis we plotted the global daily residue, i.e., the average of all the residue measurements performed by SCIAMACHY on a particular day. This global daily residue is given for the sixteen positions of

the scan mirror that are related to the integration time (IT) of 0.25 s. The result for the most westerly scan mirror position deviates by roughly 1.2 index point from the other scan mirror positions for data until the end of March, 2003.

For each of the two wavelengths, and for each of the possible ITs (0.25, 0.50, or 1.00 s; see Table 1), a different set of correction factors was determined. The resulting corrections are only to be applied to the reflectances measured by SCIAMACHY for the westernmost pixels in a scan (that is, one forward and one backward scan pixel). The correction is not applied to ‘narrow swath’ data, ‘nadir pointing-left’ data, and ‘nadir static’ data, with the exception of nadir static data in the extreme west-viewing direction. For this rare case, other correction factors are used, and applied to all measurements.

4.3 Correction for instrument degradation

The residue had increased by more than 7 index points over the last nine years (cf. Figure 5), and a recent analysis indicated that this increase was mainly caused by degradation of the optics [16]. Instrument degradation is being recorded by instrument Light Path Monitoring (LPM) measurements [18], with the eventual aim to calculate a correction to the radiometric calibration of both the radiance and irradiance. The resulting correction factors are called m-factors, and they have to be applied in the level-1b to level-1c calibration step. As of SC-AAI version 3.1, the official m-factor correction was part of the SC-AAI calibration scheme. This approach has been abandoned as of version 5.0.

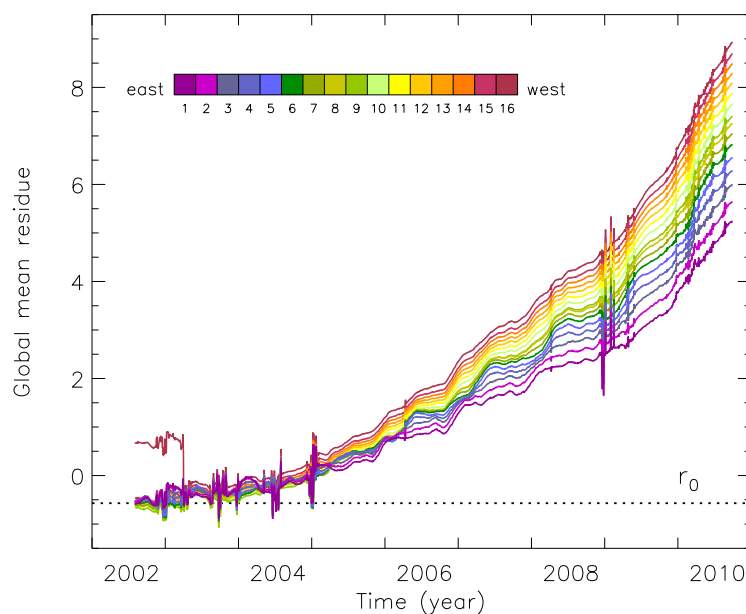


Figure 5: The globally averaged residue increased by more than 7 index points over the last nine years because of instrument degradation. The dotted line indicates the expected value r_0 .

The correction for instrument degradation currently follows a two-step approach. The approaches that were used for previous versions of the SC-AAI algorithm are also listed.

Step 1 [version 2.3 & 3.0]

To correct for instrument degradation, we make use of the so-called “White Light Source via ESM mirror” (in short: WLS) monitoring data, which should give an indication of the degradation of the nadir radiance. Alternatively, we can also make use of the so-called “Sun through subsolar port via ESM mirror, fast sweep” (in short: FS) monitoring data. Both should, in an ideal situation, record the same nadir radiance degradation. But in practice, there are large differences found. At this point in time, it is not yet clear which of the two records is the preferred one.

Finally, the daily solar irradiance measurements record a time series of the irradiance degradation. Combining this with the WLS or FS monitoring data, we can calculate the (measured) degradation in the reflectance signal. In our retrieval code, we correct the reflectances at 340 and 380 nm with multiplicative correction factors d_{340} and d_{380} , respectively. These factors have to be scaled to unity for 23 August 2002, the day for which the reflectance correction constants c_{340} and c_{380} (see previous section) were determined [14]. This correction removes most of the effects of degradation, yet some deviation Δr_0 from the expected globally average residue value r_0 remains present.

Step 1 [versions 3.1 – 4.1]

To correct for the effects of instrument degradation, we rely on the official m-factor calibration correction [19]. As explained in Section 1.3, the `sciamnl1` tool will perform this degradation/calibration correction for us upon request, when it is permitted access to the m-factor data set. The most recent version of the m-factor database at the time of writing was version 6.01. The m-factor correction removes a large portion of the degradation, but not everything. Some deviation Δr_0 from the expected globally average residue value r_0 remains present. In particular, the growing scan-angle dependence, as seen in Figure 5, is not removed, because m-factors are scan-angle independent by definition.

Step 1 [version 5.0]

The first step consists of monitoring the global mean reflectance at 340 and 380 nm in the way it was done in reference [20]. The time series of the global mean reflectance are fitted with a combination of a finite Fourier series and a polynomial base. The Fourier terms describe the seasonal variation and are disregarded because they do not contain any information about the inflicted instrument degradation. The polynomial base, on the other hand, directly describes the change in reflectance due to instrument degradation. From these the coefficients d_{340} and d_{380} are calculated.

Step 2 [versions 2.3 – 4.1]

In the next step in of the correction process, we remove the deviation Δr_0 , which we believe to be unphysical, by assuming that the global average of the residue over the globe r_0 should be constant in

time, and equal to the value reached at the start of the mission. To achieve this, we apply a correction factor d_{340} to the measured reflectance at 340 nm in such a way that the resulting change in the residue Δr , which can be calculated in an exact way using Eq. 12, exactly equals $-\Delta r_0$. As of version 3.1, this is done for each individual scan-angle position and integration time.

In summary, in the SC-AAI retrieval algorithm, we currently first apply the official m-factor correction, after which we apply a second correction, performed only on the measured reflectance at 340 nm, to remove remaining deviations from the residue. This procedure is done for each individual scan-angle position, for each integration time, and for every complete day of data. Care is taken not to interpret statistical outliers as a form of instrument degradation.

Step 2 [version 5.0]

In this step of the correction process, we apply the correction factors d_{340} and d_{380} found in “step 1” to the reflectances at 340 and 380 nm, respectively. Note that in order to obtain the correction factors, the entire SCIAMACHY database needs to be processed. In practice, this involves a post-processing step on the first run from which the coefficients were determined. Details are described in [20].

5 Filtering and flagging

Filtering is of course done prior to calculation of surface height, ozone column, and residue, in order to reduce computational time. Quality flags are available. The pixel index number, which indicates for each state the chronological order in which the measurements were performed, is made negative for backscan pixels to distinguish them from forward scan measurements.

5.1 Integration time

All states having an integration time (IT) for cluster 9 (320–391 nm) that is larger than 1.0 s are filtered out because they do not provide much useful information due to the extreme size of the measurement footprints. Apart from this, these long ITs are usually accompanied by high solar zenith angles, where the simulated reflectances are meaningless any way.

The integration time is determined from the STATES field inside the SCIAMACHY level-1c product. In certain cases this is not adequate, for instance, when (a) the STATES field does not exist, (b) the state in question is missing from the STATES field, or (c) the start time of the state is wrong as there are several states pointing to the same start time.

For these rare cases, we make use of Table 1 to manually correct the integration time on the basis of the number of measurements that is reported for cluster 9. This approach only works for nominal states, for which the number of measurements is as listed in Table 1.

measurements	state duration	integration time	exists
8	80	10.0	+
13	65	5.0	-
16	80	5.0	-
65	65	1.0	+
80	80	1.0	+
130	65	0.5	+
160	80	0.5	-
260	65	0.25	+
320	80	0.25	-
520	65	0.125	-
640	80	0.125	-

Table 1: The possible (nominal) state properties for cluster 9. The last column indicates whether the situation in question can be found in real life (+) or not (-).

5.2 Backscan pixels

Backscan pixels are identified in the following way. First, it is verified that the number of observations in a state is equal to one of the numbers in the first column of Table 1. If this is indeed the case, then we are most likely dealing with a nominal situation, and we can determine the scanning direction inside the state using the fact that the measurements are taken in the normal scanning pattern.

If this is not the case, for instance when dealing with incomplete states, we use another means of identification which relies on the sign of the third component of the cross product of the two vectors in the latitude/longitude plane that start at corner 1 and end at corner 2 and 4, respectively.

The pixel index number, which indicates for each state the order in which the measurements were performed, is made negative for backscan pixels, in order to distinguish them from forward scan measurements. Backscan pixels are not present in the data available on the TEMIS site, because they add little additional information. Exceptions are monitoring states, for which pixels that were tagged as “backscan pixels” are never filtered out, because they are no different than the pixels that were tagged differently. The sign of the pixel index number has no real meaning for these special states.

5.3 Solar zenith angle

Situations with extremely high solar zenith angles are filtered out. The maximum allowed solar zenith angle is currently set to 85°. The residues for higher solar zenith angles are meaningless.

5.4 Sunlint situations

Sunlint is caused by specular reflection of direct sunlight off the ocean’s surface. If the ocean would be a perfect mirror, sunlint would only occur in the principal plane, where $\phi = \phi_0$, and only for the specific situation where the viewing zenith angle θ and the solar zenith angle θ_0 are equal. In reality, the roughness of the ocean surface smears out the sunlint beam to some degree, and we need to define a less strict criterion to filter out possible sunlint situations.

We define the sunlint deviation angle $\Delta\Psi_{\text{glint}}$ as the deviation, in degrees, from the exact sunlint geometry. The angle may be calculated by

$$\cos \Delta\Psi_{\text{glint}} = \cos \theta \cos \theta_0 + \sin \theta \sin \theta_0 \cos (\phi - \phi_0), \quad (13)$$

where the angles involved were defined in Figure 1 and recalculated according to Section 3.4.

In the AAI retrieval code, the sunlint deviation angle $\Delta\Psi_{\text{glint}}$ is calculated for each individual SCIA-MACHY pixel. For pixels having angles $\Delta\Psi_{\text{glint}}$ below 22°, a surface type database is used to deter-

mine whether these pixels are above land or ocean surface. Those pixels that are found to be above ocean surface are likely to be the victim of sunglint and are subject to the next test.

The next step in the screening process was first introduced in SC-AAI version 4.1. Based on the available SCIAMACHY FRESCO cloud information we determine whether the sea surface was perhaps shielded off by a thick cloud. If this is the case, sunglint cannot possibly have played an important role, and the pixel is considered to be not affected by sunglint, and flagged accordingly. If the cloud cover is not thick enough, or the pixel is cloud-free, then the pixel is flagged as a possible sunglint pixel. Thick enough in this case means: cloud fraction above 0.35 and cloud pressure below 850 hPa. The latter condition is to ensure that we are really dealing with a cloud.

5.5 Solar eclipse events

Solar eclipse events lead to anomalous high values of the residue. Observations taken during a solar eclipse should not be used. The quality flag, described in Section 5.7, is set to indicate the occurrence of such situations. The flag is set according to the information given in Table 2 of Appendix B.

5.6 Reflectances and residues

There is no filtering performed on the reflectances. No filtering is performed on the residues.

5.7 Quality flags

The level-2 SC-AAI data product provides a quality flag for each measurement. The flag is given as a three-digit number (for example: “023”). Each digit refers to a specific sub-flag. The first digit indicates whether the pixel was affected by a solar eclipse event. A digit “0” indicates that the pixel was not affected. A digit “1” indicates that the pixel was most likely not affected, but that other parts of the orbit were affected. A digit “2” indicates that the pixel was definitely affected, and not to be used. Note that these events happen rarely, on average once or twice per year.

The second digit indicates the origin of the ozone column that was used. A value of “0” indicates the normal situation in which SCIAMACHY TOSOMI total ozone columns were available. If the flag is raised to “1”, then assimilated SCIAMACHY total ozone values were used as back-up. If the flag is set to “2”, then ozone information was not available for some reason and a fixed standard ozone column of 334 DU was used. The latter situation should not occur in practice.

The third digit corresponds to the outcome of the sunglint test. If the flag is set to “1”, then the scattering geometry was such that sunglint could not have occurred, in other words, $\Delta\Psi_{\text{glint}} > 22^\circ$.

If the flag is set to “2”, then the scattering geometry would have enabled sunglint to occur, i.e., $\Delta\Psi_{\text{glint}} \leq 22^\circ$, but the scene was over land. If the flag is set to “3”, then the sunglint scattering condition was met, the scene was over sea, yet covered by a thick cloud, preventing sunglint to occur. If the flag is set to “9”, then the pixel is regarded as a likely candidate for sunglint. A flag set to “8” indicates that the sunglint check was not switched on, but this flag should not occur in practice.

A Readme file delivered with look-up tables

Short description of the look-up tables (LUTs).

A. General.

The look-up tables (LUTs) were calculated using the polarised radiative transfer code DAK ("Doubling-Adding KNMI"), which is described in detail in Ref. [1]. The main features of the code are multiple scattering and a full implementation of (linear) polarisation, which is an essential ingredient for LUTs meant for the Absorbing Aerosol Index (AAI) retrieval.

This particular version of the LUTs was calculated with DAK v3.1.1. This version of DAK manages a pseudo-spherical treatment of its model atmosphere. Note that this improvement is only relevant for solar zenith angles above, say, 60 degrees.

The surface albedo A_s was set to zero in all calculations. Clouds and aerosols were not present in the model atmospheres, and a standard Mid-Latitude Summer (MLS) atmospheric profile with a surface pressure of 1013 hPa at sea level was used in all calculations. For taking surface pressure into account, the LUTs were calculated for surface heights of

$z = 0$ km	$p_0 = 1013$ hPa	(=sea level)
$z = 1$ km	$p_0 = 902$ hPa	
$z = 2$ km	$p_0 = 802$ hPa	
$z = 3$ km	$p_0 = 710$ hPa	
$z = 4$ km	$p_0 = 628$ hPa	
$z = 5$ km	$p_0 = 554$ hPa	
$z = 6$ km	$p_0 = 487$ hPa	
$z = 7$ km	$p_0 = 426$ hPa	
$z = 8$ km	$p_0 = 372$ hPa	

The different surface heights were modelled by physically removing layers from the bottom of the model atmosphere.

The DAK code can also deal with absorption by molecules. Only ozone absorption was taken into account. A standard Mid-latitude Summer (MLS) profile was used, and the ozone profiles were scaled so as to let the ozone column reach its intended value.

The LUTs were calculated for 7 ozone columns, ranging between 50 and 650 Dobson Units (DU).

The following table lists the ozone column values used:

o = 0	O3 = 50 DU
o = 1	O3 = 200 DU
o = 2	O3 = 300 DU
o = 3	O3 = 350 DU
o = 4	O3 = 400 DU
o = 5	O3 = 500 DU
o = 6	O3 = 650 DU

Viewing and solar zenith angles are available for 42 different angles between 0 and 90 degrees. All calculations were performed for a relative azimuth of 0 degrees.

B. Format of LUT files.

The files have names like "aailut340_z2_o3". The first number relates to the wavelength (340 nm in this case). The second number relates to the surface height. A zero indicates sea level; 8 refers to a surface height of 8 km. The third number shows the ozone column used. A zero indicates 50 DU, 6 refers to an ozone column of 650 DU; see table above.

Inside the file, we find:

- a) the number of Fourier coefficients, which is always 3
- b) the number of Gaussian mu-points, which is always 42
- c) the wavelength (in units of nanometers)
- d) the surface pressure p_0 (in units of hPa)
- e) the ozone column O3 (in DU)
- f) s^*
- g) μ
- h) $T(\mu, \mu_0)$
- i) $a_0(\mu, \mu_0)$
- j) $a_1(\mu, \mu_0)$
- k) $a_2(\mu, \mu_0)$

The matrix $T(\mu, \mu_0)$ is the so-called transmission matrix, which could normally be written as a product of the transmissions functions $t(\mu)$ and $t(\mu_0)$, as described in Ref. [2]. However, because of the use of a semi-spherical RTM, there is symmetry breaking between the viewing and solar directions and $T(\mu, \mu_0)$ cannot be described as such a product any more. For that reason, the entire matrix is given.

The number of Fourier coefficients is always equal to three (we have a_0 , a_1 , and a_2). The number of gaussian μ -points is 42 in all provided files.

The coefficients a_0 , a_1 , and a_2 are defined as in Ref. [2].

That is, the reflectance may be calculated from them according to

$$R_0 = a_0 + 2 * a_1 * \cos(\phi - \phi_0) + 2 * a_2 * \cos^2(\phi - \phi_0)$$

This procedure is also explained in Ref. [2].

As a final note, please note that the matrices T , a_0 , a_1 , and a_2 have been made symmetrical in μ and μ_0 by mirroring. Therefore, accidental swapping of the μ and μ_0 parameters should not have an effect.

C. References.

[1]

de Haan, J.F., P.B. Bosma, and J.W. Hovenier (1987), The adding method for multiple scattering calculations of polarised light, *Astron. Astrophys.*, 183, 371-391.

[2]

de Graaf M., P. Stammes, O. Torres, and R.B.A. Koelemeijer (2005), Absorbing Aerosol Index: Sensitivity analysis, application to GOME and comparison with TOMS, *J. Geophys. Res.*, 110, D01201, doi:10.1029/2004JD005178.

L.G. Tilstra (KNMI)

e-mail: tilstra@knmi.nl

B Overview of solar eclipse events

The following table provides an overview of the major solar eclipse events that have occurred since the launch of Envisat in March 2002. The first column lists the dates on which the solar eclipse event occurred, the second column lists the orbits which were affected. Usually one orbit is affected. The time interval in which the measurements were affected is found in the third and fourth column.

date	orbit	start time	end time
31-MAY-2003	06529	04:49:36 UTC	05:06:01 UTC
23-NOV-2003	09058	21:57:21 UTC	21:58:25 UTC
14-OCT-2004	13713	02:00:47 UTC	02:16:13 UTC
08-APR-2005	16242	18:45:50 UTC	19:08:01 UTC
03-OCT-2005	18784	08:33:18 UTC	08:40:35 UTC
03-OCT-2005	18785	10:12:58 UTC	10:22:20 UTC
29-MAR-2006	21318	09:15:00 UTC	09:24:22 UTC
22-SEP-2006	23853	11:40:43 UTC	11:52:09 UTC
19-MAR-2007	26396	03:00:21 UTC	03:07:38 UTC
11-SEP-2007	28921	13:07:23 UTC	13:21:06 UTC
01-AUG-2008	33572	10:23:53 UTC	10:40:19 UTC
26-JAN-2009	36117	06:07:35 UTC	06:23:10 UTC
22-JUL-2009	38648	01:24:19 UTC	01:37:49 UTC
15-JAN-2010	41184	05:34:18 UTC	05:45:44 UTC
11-JUL-2010	43725	18:00:10 UTC	18:05:22 UTC
04-JAN-2011	46257	08:35:18 UTC	08:51:35 UTC

Table 2: Solar eclipse events since the launch of Envisat. Date and orbit number of the affected orbits are given, as well as the time interval in which the measurements were noticeably affected.

References

- [1] Bovensmann, H., J. P. Burrows, M. Buchwitz, J. Frerick, S. Noël, V. V. Rozanov, K. V. Chance, and A. P. H. Goede (1999), SCIAMACHY: Mission objectives and measurement modes, *J. Atmos. Sci.*, 56(2), 127–150.
- [2] Slijkhuis, S. (2001), SCIAMACHY level 0 to 1c processing algorithm theoretical basis document, *Tech. Note ENV-ATB-DLR-SCIA-0041*, Dtsch. Zent. für Luft- und Raumfahrt, Oberpfaffenhofen, Germany.
- [3] NADC tools homepage; software from the Netherlands SCIAMACHY Data Center (NL-SCIADC), <http://www.sron.nl/~richardh/SciaDC/>.
- [4] Bramstedt, K. (2008), Calculation of SCIAMACHY m-factors, *Tech. Note IFE-SCIA-TN-2007-01-CalcMFactor*, Issue 1, April 1, 2008.
- [5] Burrows, J. P., et al. (1999), The Global Ozone Monitoring Experiment (GOME): Mission concept and first scientific results, *J. Atmos. Sci.*, 56(2), 151–175.
- [6] Herman, J. R., P. K. Bhartia, O. Torres, C. Hsu, C. Seftor, and E. Celarier (1997), Global distributions of UV-absorbing aerosols from Nimbus 7/TOMS data, *J. Geophys. Res.*, 102(D14), 16,911–16,922, doi:10.1029/96JD03680.
- [7] Torres, O., P. K. Bhartia, J. R. Herman, Z. Ahmad, and J. Gleason (1998), Derivation of aerosol properties from satellite measurements of backscattered ultraviolet radiation: Theoretical basis, *J. Geophys. Res.*, 103(D14), 17,099–17,110, doi:10.1029/98JD00900.
- [8] Herman, J. R., and E. A. Celarier (1997), Earth surface reflectivity climatology at 340–380 nm from TOMS data, *J. Geophys. Res.*, 102(D23), 28,003–28,011, doi:10.1029/97JD02074.
- [9] de Graaf, M. (2006), Remote Sensing of UV-absorbing aerosols using space-borne spectrometers, Ph.D Thesis, Vrije Universiteit Amsterdam, Amsterdam, 132p.
- [10] Chandrasekhar, S. (1960), *Radiative Transfer*, Dover, Mineola, N. Y., 393p.
- [11] de Haan, J. F., P. B. Bosma, and J. W. Hovenier (1987), The adding method for multiple scattering calculations of polarized light, *Astron. Astrophys.*, 183, 371–391.
- [12] Anderson, G. P., S. A. Clough, F. X. Kneizys, J. H. Chetwynd, and E. P. Shettle (1986), AFGL atmospheric constituent profiles (0–120 km), *Environ. Res. Pap. 954, Rep. AFGL-TR-86-0110*, Air Force Geophys. Lab., Hanscom AFB, Mass.

- [13] U.S. Department of Commerce, National Oceanic and Atmospheric Administration, National Geophysical Data Center (2006), *2-minute Gridded Global Relief Data (ETOPO2v2)*, <http://www.ngdc.noaa.gov/mgg/fliers/06mvg01.html>
- [14] Tilstra, L. G., G. van Soest, and P. Stammes (2005), Method for in-flight satellite calibration in the ultraviolet using radiative transfer calculations, with application to Scanning Imaging Absorption Spectrometer for Atmospheric Chartography (SCIAMACHY), *J. Geophys. Res.*, *110*, D18311, doi:10.1029/2005JD005853.
- [15] Tilstra, L. G. (2009), A recipe to convert remote sensing viewing and solar angles at the satellite into the angles at sea level, KNMI Internal Memo, July 23, 2009.
- [16] Tilstra, L. G., M. de Graaf, S. Noël, I. Aben, and P. Stammes (2007), SCIAMACHY's Absorbing Aerosol Index and the consequences of instrument degradation, in *Proceedings of the third Workshop on the Atmospheric Chemistry Validation of Envisat*, *Eur. Space Agency Spec. Publ. SP-642*, edited by D. Danesy, ESA Publications Division, Noordwijk, The Netherlands.
- [17] de Graaf, M., and P. Stammes (2002), First verification of SCIAMACHY's absorbing aerosol index product, in *Proceedings of the Envisat Validation Workshop*, *Eur. Space Agency Spec. Publ. SP-531*, edited by H. Sawaya-Lacoste, ESA Publications Division, Frascati, Italy.
- [18] Noël, S., H. Bovensmann, K. Bramstedt, J. P. Burrows, M. Gottwald, and E. Krieg (2006), SCIAMACHY Light Path Monitoring Results, in *Proceedings of the first Atmospheric Science Conference*, *Eur. Space Agency Spec. Publ. SP-628*, edited by H. Lacoste, ESA Publications Division, Noordwijk, The Netherlands.
- [19] SCIAMACHY m-factors homepage; <http://www.iup.uni-bremen.de/sciamachy/mfactors/>.
- [20] Tilstra, L. G., M. de Graaf, I. Aben, and P. Stammes (2011), In-flight degradation correction of SCIAMACHY UV reflectances and Absorbing Aerosol Index, *J. Geophys. Res.*, submitted.